

# Can the early X-ray afterglow of GRBs be explained by a contribution from the reverse shock?

F. Genet, F. Daigne & R. Mochkovitch

*Institut d'Astrophysique de Paris - UMR 7095 CNRS et Université Pierre et Marie Curie,*

*98 bis, boulevard Arago, 75014 Paris, France*

e-mail: mochko@iap.fr

13 December 2007

## ABSTRACT

We propose to explain the recent observations of GRB early X-ray afterglows with SWIFT by the dissipation of energy in the reverse shock which crosses the ejecta as it is decelerated by the burst environment. We compute the evolution of the dissipated power and discuss the possibility that a fraction of it can be radiated in the X-ray range. We show that this reverse shock contribution behaves in a way very similar to the observed X-ray afterglows if the following two conditions are satisfied: (*i*) the Lorentz factor of the material which is ejected during the late stages of source activity decreases to small values  $\Gamma < 10$  and (*ii*) a large part of the shock dissipated energy is transferred to a small fraction ( $\zeta \lesssim 10^{-2}$ ) of the electron population. We also discuss how our results may help to solve some puzzling problems raised by multiwavelength early afterglow observations such as the presence of chromatic breaks.

**Key words:** gamma ray: bursts; shock waves; radiation mechanisms: non-thermal

## 1 INTRODUCTION

The X-Ray Telescope (XRT) on board the SWIFT satellite has for the first time allowed a follow-up of the X-ray afterglows of GRBs starting within one minute of the BAT trigger (Burrows et al. 2005a). These early afterglow observations have revealed several surprising features which cannot be easily understood in terms of the usual interpretation where the afterglow comes from dissipation in a forward shock propagating through the source envi-

ronment. At very early times immediately after the burst prompt emission, the afterglow first exhibits a steep decrease of temporal slope  $\alpha_1 \sim 3 - 5$  ( $F_X \propto t^{-\alpha}$ ) (Tagliaferri et al. 2005). It is often followed by a much shallower part with  $0.2 < \alpha_2 < 0.8$  which can last for several hours until a more standard slope  $1 < \alpha_3 < 1.5$  is finally observed (Nousek et al. 2005). Moreover flares with sharp rise and decay times are often present, superimposed on the power-law evolution (Burrows et al. 2005b). In most cases, the spectrum remains essentially constant through the breaks which may indicate that a single physical process is responsible for the whole X-ray emission. The forward shock could be such a process but it seems unable, at least in its simplest version, to account for the early slopes  $\alpha_1$  and  $\alpha_2$ . It has been suggested that the shallow part of the light curve could still be produced by the forward shock if it is continuously feeded in energy by the central source (Panaitescu et al. 2005; Zhang et al. 2005). Another possibility would be to delay the rise of the forward shock contribution as a result of viewing angle effects (Eichler and Granot, 2005). These two proposals would however strengthen the constraint on the efficiency of the prompt gamma-ray emission which is already a potential problem for the internal shock scenario (see however Fan & Piran, 2006 and Zhang et al. 2006). For the initial steep decay, curvature effects of the emitting shell have been invoked (Nousek et al. 2005) while flares are usually explained by a late activity of the central source (Zhang et al. 2005; Fan & Wei, 2005).

In this paper we do not consider the origin of flares but rather focus on the evolution of the early X-ray afterglow. We propose that it could be accounted for by a contribution from the reverse shock. We develop a simple model which allows us to follow the internal, reverse and forward shocks in a consistent way. We compute the energy dissipated in the reverse shock and show that, for some specific initial distribution of the Lorentz factor in the flow, it is possible to reproduce the succession of the three slopes  $\alpha_1$ ,  $\alpha_2$  and  $\alpha_3$ . We then discuss under which conditions part of this dissipated energy can be radiated in the X-ray range, providing an alternative explanation for the early X-ray afterglows of GRBs. We also obtain the optical emission of the reverse shock and show that chromatic breaks can be observed in some cases.

The paper is organized as follows: in Sect.2 we present the simplified model we use to follow the dynamics of internal shocks. We explain in Sect.3 how it is extended to include the interaction with the environment and we compute the power dissipated in the reverse shock. We consider in Sect.4 the possibility for this power to be partially radiated in the X-ray range. We discuss in Sect.5 the relative importance of the reverse and forward shock

contributions and present X-ray and optical afterglow light curves produced by the reverse shock alone. Sect.6 is our conclusion.

## 2 THE ORIGIN OF GRB PULSES

In the context of the internal shock model for the prompt emission of GRBs the pulses observed in the light curve are produced when fast moving material catches up with slower one previously ejected by the central source (Rees & Meszaros, 1994). This process has often been represented by the collision of two “shells” of negligible thickness. However the central source probably does not release individual shells but a continuous relativistic outflow with a varying Lorentz factor. For this reason the shape of the pulses is largely dominated by hydrodynamical effects (Daigne & Mochkovitch, 2003) while high latitude emission (curvature effect) only becomes important at late times. Soderberg and Fenimore (2001) have for example found that the decay of pulses differs from what would be expected if it was controlled by the curvature effect alone. A hydrodynamical study of the relativistic flow emerging from the central engine therefore appears necessary for a detailed description of the physics of pulses but it is naturally quite expensive in computing time (Daigne & Mochkovitch, 2000). Fortunately it can often be replaced by a simplified model where the flow is represented by a large number of regularly ejected shells which interact by direct collision only (Daigne & Mochkovitch, 1998). This neglects pressure waves but this is a good approximation since kinetic energy strongly dominates over internal energy of the flow. This approach implies to use many shells (from  $10^3$  to  $10^4$ ) to represent accurately the distribution of mass and Lorentz factor. It is different from the even more simplified description where the numbers of shells essentially corresponds to the number of pulses to be produced and where the temporal profiles are then entirely fixed by the curvature effect (Kobayashi, Piran & Sari, 1997).

The position  $R_i$  of each shell of mass  $M_i$  and Lorentz factor  $\Gamma_i$  is followed as a function of time  $t$  (in the source frame). When shell  $i$  catches up with shell  $i + 1$  a shock occurs at time  $t_s$  and radius  $R_s$ . The two shells merge and the resulting Lorentz factor after the collision is given by

$$\Gamma_r = \sqrt{\Gamma_i \Gamma_{i+1} \frac{m_i \Gamma_i + m_{i+1} \Gamma_{i+1}}{m_i \Gamma_{i+1} + m_{i+1} \Gamma_i}}. \quad (1)$$

If the the released energy

$$E = m_i \Gamma_i c^2 + m_{i+1} \Gamma_{i+1} c^2 - (m_i + m_{i+1}) \Gamma_r c^2 \quad (2)$$

can be efficiently radiated it will be received by the observer at a time

$$t_{\text{obs}} = t_s - \frac{R_s}{c} \quad (3)$$

and for a typical duration

$$\Delta t_{\text{obs}} = \frac{R_s}{2c\Gamma_r^2} \quad (4)$$

under the condition that the radiative time is much smaller than the dynamical time (fast cooling regime). The burst bolometric luminosity can then be obtained from the sum of all the elementary shock contributions, the dynamical evolution being terminated when all the shells have their Lorentz factor decreasing downstream so that no new internal shock can form. For an accurate description of the pulse profile at late times, the contribution  $\ell(t)$  of each elementary shock must include the curvature effect of the emitting shell which yields

$$\ell(t) = \frac{2E}{\Delta t_{\text{obs}} \left(1 + \frac{t-t_{\text{obs}}}{\Delta t_{\text{obs}}}\right)^3} \quad (5)$$

for  $t_{\text{obs}} < t < t_{\text{obs}} + (1 - \cos\Delta\theta) R_s/c$ , where  $\Delta\theta$  is the opening angle of the jet here supposed to be seen on axis (Granot, Piran & Sari, 1999; Woods & Loeb, 1999). The luminosity in a given energy band depends on some additional (and uncertain) assumptions on the post-shock magnetic field and Lorentz factor of the electrons which are discussed in Sect. 4 and 5 while in Sect. 3 we restrict ourselves to the bolometric emission only.

To produce a single pulse burst (or a pulse as a building block of a more complex burst) we have often used in previous works (Daigne & Mochkovitch, 1998, 2000) an initial distribution of the Lorentz factor of the form

$$\Gamma(t) = \frac{\Gamma_{\text{max}} + \Gamma_{\text{min}}}{2} - \frac{\Gamma_{\text{max}} - \Gamma_{\text{min}}}{2} \cos\left(\pi \frac{t}{0.2 t_W}\right) \quad (6)$$

if  $t < 0.2 t_W$  and  $\Gamma(t) = \Gamma_{\text{max}}$  if  $t > 0.2 t_W$ ;  $\Gamma_{\text{max}}$  and  $\Gamma_{\text{min}}$  are the maximum and minimum values of the Lorentz factor and  $t_W$  the duration of the relativistic wind emission (the first shell is then ejected at  $t = 0$  and the last one at  $t = t_W$ ). This Lorentz factor distribution where a rapid part of the flow is decelerated by a slower part placed ahead of it, has been represented in Fig.1a for  $\Gamma_{\text{max}} = 200$ ,  $\Gamma_{\text{min}} = 50$  and  $t_W = 10$  s. The resulting bolometric profile from dissipation by internal shocks is shown in Fig.1b for a total (isotropic) radiated energy  $E_{\text{rad}} = 10^{53}$  erg.

The decline of the pulse after maximum is first controlled by the dynamics of internal shocks. This would lead to an asymptotic behavior  $L(t) \propto t^{-3/2}$  if it was not interrupted

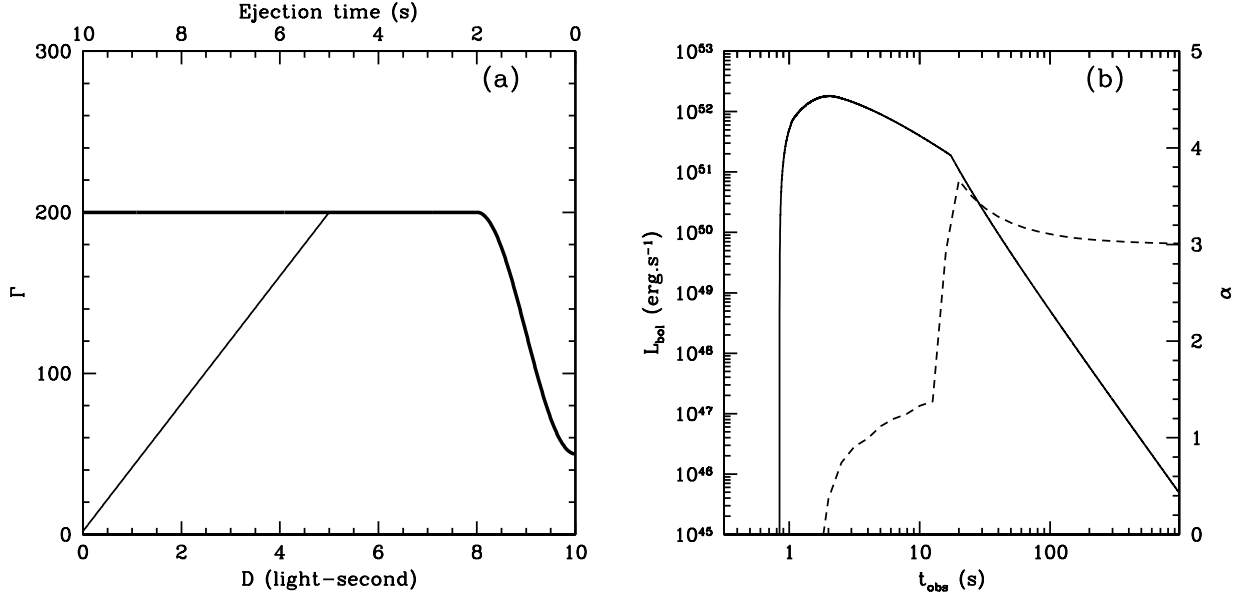


**Figure 1.** A single pulse burst. (a): Initial distribution of the Lorentz factor in the relativistic flow as a function of ejection time and distance  $D$  to the source (in light-seconds) according to Eq.(6) with  $\Gamma_{\max} = 200$ ,  $\Gamma_{\min} = 50$  and  $t_W = 10$  s (thick full line) and to Eq.(7) with  $\delta = 1$  and  $\Gamma_f = 2$  (thin full line); (b): Bolometric profile for the distribution given by Eq.(6) (full line) together with the corresponding temporal slope  $\alpha$  (dashed line). After maximum, the profile is first controlled by the dynamics of internal shocks before the curvature effect eventually dominates after  $t_{\text{obs}} \sim 20$  s.

at a time  $\tau \sim t_W$  when all the fast material of the ejecta has been shocked. Daigne and Mochkovitch (2003) have shown that the gamma-ray profiles which can be obtained from this first part of the bolometric light curve are generally in good agreement with the early decline following maximum count rate in observed GRBs (Ryde & Svensson, 2000).

After all the ejecta has been shocked the pulse evolution becomes fixed by geometry, the contribution of each shocked shell being given by Eq.(5). At large times  $t \gg \tau$ , all the  $\ell(t)$  and therefore the global profile  $L(t)$  asymptotically behave as  $t^{-3}$ . However at early times  $t \gtrsim \tau$ , a steeper decline can be obtained (Nousek et al. 2005) as illustrated in Fig.1b where the temporal slope  $\alpha$  has been plotted together with the profile. It has a maximum of 3.65 just at the end of the internal shock phase before relaxing to 3 after a few  $\tau$ .

### 3 THE REVERSE SHOCK

#### 3.1 Physical description

The profile calculated above corresponds to a “naked GRB” (Kumar & Panaitescu, 2000) and would be the only component observed in the absence of external medium. The burst environment will however interact with the ejecta, leading to a forward shock propagating through the circumstellar medium and a reverse shock sweeping back into the ejecta. We

compute below (Sect.3.2) the power dissipated in the reverse shock and discuss its possible contribution to the early X-ray emission of GRBs. With the initial distribution of the Lorentz factor given by Eq.(6) the reverse shock crosses the ejecta in a short time and cannot explain an emission lasting for several days. The situation is however very different if a slight change is made in the initial distribution of the Lorentz factor. We expect that the central source will not stop ejecting relativistic material abruptly at  $t = t_W$ . We instead propose that  $\Gamma$  will progressively decrease until it reaches a small value (possibly close to unity) at  $t_W$ . Since  $\Gamma(t)$  is given by the ratio  $\dot{E}/\dot{M}$  of the energy to mass injection rates, a small  $\Gamma$  can be a consequence of (i) a decrease of  $\dot{E}$ , less and less energy becoming available from the source to accelerate a given baryon load or/and (ii) a catastrophic increase of  $\dot{M}$ . Case (i) appears more natural during the late stages of source activity and has been adopted in presenting our results in Sect.3.2.

We have then introduced a new distribution of the Lorentz factor where, for  $t > 0.5 t_W$ ,  $\Gamma(t)$  decreases to a final value  $\Gamma_f$

$$\Gamma(t) = \Gamma_f + (\Gamma_{\max} - \Gamma_f) \left[ \frac{1 - t/t_W}{0.5} \right]^\delta \quad (7)$$

while for  $t < 0.5 t_W$ ,  $\Gamma(t)$  is still given by Eq.(6). This modified Lorentz factor is plotted in Fig.1a for  $\Gamma_{\max} = 200$ ,  $\Gamma_f = 2$ ,  $t_W = 10$  s and  $\delta = 1$ . With this new distribution, the duration of source activity remains unchanged but the reverse shock will be present for a much longer time, until all the ejecta has been decelerated to  $\Gamma \sim \Gamma_f$ . The forward shock also remains feeded in energy as slow material from the ejecta is continuously catching up but the resulting effect is too small in this case to account for the shallow part of the light curve (we assumed that equal amounts of kinetic energy are injected before and after  $t = 0.5 t_W$ ).

To compute the energy dissipated in the reverse shock we had to implement in our shell model the interaction with the burst environment. This was done by considering the contact discontinuity which separates the ejecta and the shocked external medium. In our simple description it is represented by two shells moving at the same Lorentz factor  $\Gamma$ . The first one corresponds to the mass  $M_{ej}$  of the ejecta already crossed by the reverse shock, which carries a total energy  $\Gamma M_{ej} c^2$ , and the second to the shocked external medium of mass  $M_{ex}$ . If the forward shock moves quasi-adiabatically (slow cooling regime), this shell keeps its internal energy (since  $p dV$  work is neglected in our simple model) so that its total energy is  $\Gamma \Gamma_i M_{ex} c^2$  where  $(\Gamma_i - 1)c^2$  is the dissipated energy (per unit mass) in the fluid rest frame. Two processes will affect this two shell structure at the contact discontinuity : it will collide

either with shells of the external medium at rest, or with rapid shells of the relativistic ejecta catching up. This represents both the forward and reverse shock in our simplified picture.

*Forward shock:* the interaction with the external medium is discretized by assuming that a collision occurs each time the contact discontinuity has travelled from a radius  $R$  to a radius  $R'$  so that the swept-up mass is

$$m_{\text{ex}} = \int_R^{R'} 4\pi r^2 \rho(r) dr = q \frac{M}{\Gamma} \quad (8)$$

where  $M = M_{\text{ej}} + M_{\text{ex}}$ ,  $\rho(r)$  is the density of the external medium (for which we adopted either a constant or a stellar wind distribution) and  $q \ll 1$  (we take in practice  $q = 10^{-2}$ ).

Writing the conservation of energy-momentum for this collision, we obtain the new Lorentz factor  $\Gamma_r$  at the contact discontinuity

$$\Gamma_r = \left[ \frac{(M_{\text{ej}} + M_{\text{ex}}\Gamma_i)\Gamma^2 + m_{\text{ex}}\Gamma}{(M_{\text{ej}} + M_{\text{ex}}\Gamma_i) + 2m_{\text{ex}}\Gamma} \right]^{1/2} \quad (9)$$

and also the new Lorentz factor  $\Gamma'_i$  for internal motions after the collision

$$\Gamma'_i = \frac{(M_{\text{ej}} + M_{\text{ex}}\Gamma_i)\Gamma + m_{\text{ex}} - M_{\text{ej}}\Gamma_r}{(M_{\text{ex}} + m_{\text{ex}})\Gamma_r}. \quad (10)$$

It should be noted that the above equations assume that material in the burst environment is at rest. This neglects the pair-loading process resulting from the initial flash of gamma-rays which pre-accelerates the circumstellar medium (Madau & Thompson, 2000; Thompson & Madau, 2000; Beloborodov, 2002) out to a radius

$$R_{\text{acc}} \sim 7 \cdot 10^{15} E_{\gamma,53}^{1/2} \text{ cm} \quad (11)$$

where  $E_{\gamma,53}$  is the isotropic gamma-ray energy of the flash in units of  $10^{53}$  erg. For this reason, the deceleration by the external medium will be delayed by

$$\Delta t_{\text{acc}} \sim \frac{R_{\text{acc}}}{2c\Gamma^2} = 12 E_{\gamma,53}^{1/2} \Gamma_2^{-2} \text{ s} \quad (12)$$

where  $\Gamma_2$  is the average Lorentz factor of the ejecta in units of  $10^2$ . Therefore the initial dynamical evolution will be that of a naked GRB but the effect will last more than one minute only for the most extreme bursts with  $E_{\gamma,53} > 10$ .

*Reverse shock:* as the Lorentz factor at the contact discontinuity decreases, new shells from the ejecta become able to catch up. Writing again the conservation of energy-momentum for these collisions, we obtain the change in Lorentz factor

$$\Gamma_r = \sqrt{\Gamma\gamma_{\text{ej}}} \left[ \frac{(M_{\text{ej}} + M_{\text{ex}}\Gamma_i)\Gamma + m_{\text{ej}}\gamma_{\text{ej}}}{(M_{\text{ej}} + M_{\text{ex}}\Gamma_i)\gamma_{\text{ej}} + m_{\text{ej}}\Gamma} \right]^{1/2} \quad (13)$$

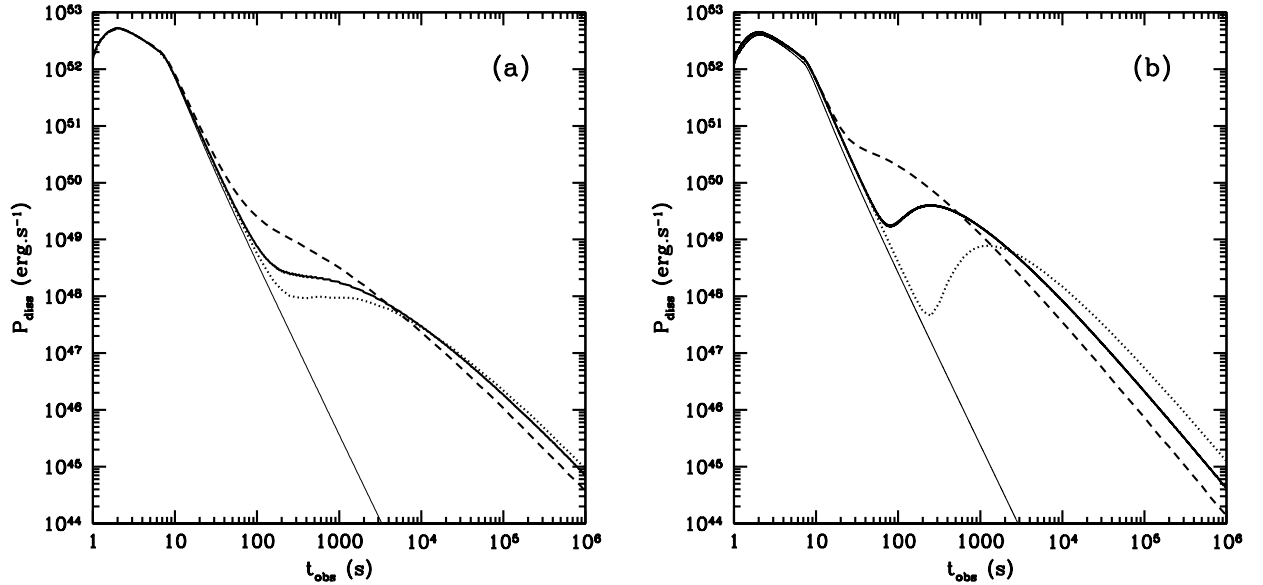


**Figure 2.** Dissipated power as a function of observer time during reverse shock propagation when the Lorentz factor is given by Eq.(7) with  $\Gamma_f = 2$  and  $\delta = 1$ . (a): wind case with  $A_* = 0.5$  (dashed line),  $A_* = 0.1$  (full line) and  $A_* = 0.05$  (dotted line); (b): uniform density case with  $n = 1000$  (dashed line), 10 (full line) and  $0.1 \text{ cm}^{-3}$  (dotted line). In each panel the thin full line represents the naked burst.

and the related dissipated energy

$$E_{\text{diss}} = (M_{\text{ej}} + M_{\text{ex}}\Gamma_i)\Gamma c^2 + m_{\text{ej}}\gamma_{\text{ej}}c^2 - (M_{\text{ej}} + m_{\text{ej}} + M_{\text{ex}}\Gamma_i)\Gamma_r c^2 \quad (14)$$

where  $m_{\text{ej}}$  and  $\gamma_{\text{ej}}$  are respectively the mass and Lorentz factor of the colliding material from the ejecta.

### 3.2 The dissipated power

Using this simplified model for the interaction of the ejecta with its environment we can describe the deceleration of the front shell and the propagation of the reverse shock. We have obtained the dissipated power in the reverse shock for different burst environments (uniform medium or wind). In the wind case, we considered three values of the parameter  $A_*$ : 0.5, 0.1 and 0.05 (such as  $\rho(r) = 5 \cdot 10^{11} A_*/r^2 \text{ g.cm}^{-3}$  with  $A_* = 1$  for a wind mass loss rate  $\dot{M}_w = 10^{-5} M_\odot.\text{yr}^{-1}$  and a terminal velocity  $v_\infty = 1000 \text{ km.s}^{-1}$ ). In the constant density case, we also tried three values of  $n$ : 1000, 10 and  $0.1 \text{ cm}^{-3}$ . The resulting profiles are shown in Fig.2 for  $\Gamma_f = 2$  and  $\delta = 1$  in Eq.(7) but we checked that they remain essentially unchanged when  $\Gamma_f$  is varied between 1 and 10 and  $\delta$  between 0.5 and 2.

The curves in Fig.2 show a striking resemblance with the early X-ray afterglows observed by SWIFT. After about 100 s the reverse shock component dominates over the tail of the of the burst prompt emission computed in the last section. At late times the decline follows a

constant slope  $\alpha \sim 1.5$ . The shape of the intermediate region is most sensitive to the density of the burst environment. At high density it is nearly suppressed, the constant slope  $\alpha \sim 1.5$  following directly the initial steep decrease. Conversely at low density, it can become completely flat and even fall to a temporary minimum. For comparison, we have also represented in Fig.2 the profile corresponding to the naked GRB. Without an external medium and for the distribution of Lorentz factor given by Eq.(7) (with  $\Gamma_f = 2$  and  $\delta = 1$ ) we find that a large fraction of the ejecta (all slow material with  $\Gamma < 140$ ) remains unaffected by internal shocks. With an external medium the reverse shock propagates through this material which produces the additional power at late times.

To elucidate the behavior of the reverse shock contribution we have considered the following simplified case which can be handled analytically: the ejecta is supposed to be made of a rapid single shell of mass  $M_0$  and initial Lorentz factor  $\Gamma_0$  (representing the fast material where the prompt emission takes place) followed by a slower tail of the form

$$\Gamma(M) = \Gamma_f + (\Gamma_0 - \Gamma_f) \left( \frac{M}{M_s} \right)^\delta \quad (15)$$

where  $\Gamma_f$  is the final Lorentz factor at the end of the tail and  $M_s$  is the total mass of the slow material ( $M = 0$  corresponds to the last emitted shell and  $\delta$  allows to vary the tail shape). Notice that this expression of  $\Gamma(M)$  directly results from Eq.(7) if  $\dot{M}$  is constant. Such a distribution of  $\Gamma$  skips the prompt phase and the resulting dissipated power  $P_{\text{diss}}$  comes from the reverse shock only.

The reverse shock contribution is maximum at a time close to the deceleration time of the front shell

$$t_{\text{dec}} = \frac{R_{\text{dec}}}{2c\Gamma_0^2} \quad \text{with} \quad R_{\text{dec}} = \left[ \frac{M_0(3-s)}{4\pi A\Gamma_0} \right]^{\frac{1}{3-s}} \quad (16)$$

where we have used the notation  $\rho = Ar^{-s}$  with  $A = \rho$  and  $s = 0$  for a uniform medium and  $s = 2$  for a stellar wind. A full analytical solution can be obtained for the reverse shock contribution but we only derive below its asymptotic behavior assuming that the front shell essentially follows the Blandford-McKee solution, i.e. it is only weakly affected by the additional energy coming from the slow material progressively catching up. We have checked this approximation with the numerical simulations and it is satisfied to an accuracy of about 25%.

We can write the power dissipated in the reverse shock as

$$P_{\text{diss}} = -\frac{dM}{d\Gamma} \frac{d\Gamma}{dt} \Gamma e c^2 \quad (17)$$

where  $t$  is the observer time when a shell of Lorentz factor  $\Gamma$  catches up with the front shell. The fraction  $e$  of the incoming material kinetic energy dissipated in the collision can be obtained from Eq.(13) and (14) with  $m_{\text{ej}} \ll M_{\text{ej}} + M_{\text{ex}}\Gamma_i$ , leading to

$$e = \frac{1}{2} \left[ 1 - \left( \frac{\Gamma_{\text{fs}}}{\Gamma} \right) \right]^2 \quad (18)$$

where  $\Gamma_{\text{fs}}$  is the Lorentz factor of the front shell given by the Blandford-McKee solution

$$\Gamma_{\text{fs}} \simeq \Gamma_0 \left( \frac{R}{R_{\text{dec}}} \right)^{-\lambda} \quad (19)$$

with  $\lambda = \frac{3-s}{2} = 3/2$  (resp.  $1/2$ ) for a uniform medium (resp. a stellar wind). Using  $dR/dt = 2c\Gamma_{\text{fs}}^2$  we then get the relation between shock radius and observer time

$$\frac{t}{t_{\text{dec}}} = \frac{1}{2\lambda + 1} \left( \frac{R}{R_{\text{dec}}} \right)^{2\lambda+1} . \quad (20)$$

With our assumed distribution (Eq.(15)) of the Lorentz factor in the slow material which is steadily increasing outwards, each shell moves independently at the constant Lorentz factor  $\Gamma$  until it catches up with the forward shock. We moreover neglect the fact that the slow material is emitted over a certain duration and we write the position of each shell as a function of observer time as

$$\frac{R}{R_{\text{dec}}} = \frac{t}{t_{\text{dec}}} \left( \frac{\Gamma}{\Gamma_0} \right)^2 . \quad (21)$$

Notice that if the Lorentz factor is not initially monotonic in the slow material, internal shocks will take place which, when they are completed, will leave a new distribution of  $\Gamma$ , now steadily increasing outwards. For observing times long compared to the time of internal shocks Eq.(21) will therefore still hold.

Eliminating the radius between Eq.(20) and (21) gives the time when a shell of Lorentz factor  $\Gamma$  catches up with the forward shock

$$\frac{t}{t_{\text{dec}}} = (2\lambda + 1)^{1/2\lambda} \left( \frac{\Gamma}{\Gamma_0} \right)^{-\frac{2\lambda+1}{\lambda}} . \quad (22)$$

Now from Eq.(19), (20) and (22) we can obtain the Lorentz factor  $\Gamma_{\text{fs}}$  of the forward shock when the slow shell of Lorentz factor  $\Gamma$  catches up

$$\Gamma_{\text{fs}} = \Gamma (2\lambda + 1)^{-1/2} . \quad (23)$$

To end with a simple power law expression for the dissipated power we write

$$\frac{dM}{d\Gamma} = \frac{M_s}{\delta \Gamma_0} \left( \frac{\Gamma}{\Gamma_0} \right)^{\frac{1-\delta}{\delta}} \quad (24)$$

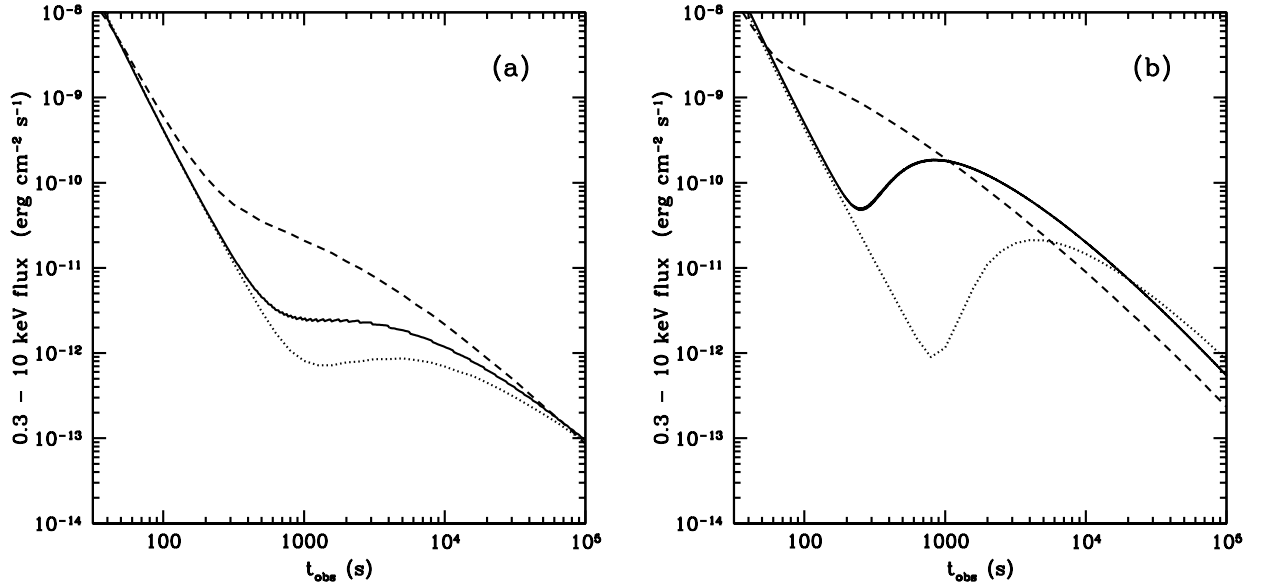


**Figure 3.** Synthetic X-ray light curves in the 0.3 - 10 keV range for the models of Fig.2. The adopted post-shock energy redistribution parameters are  $\epsilon_e = \epsilon_B = 1/3$  and  $\zeta = 10^{-2}$ . The assumed burst redshift is  $z = 2$ ; The different cases considered in Fig.2 are represented by the same full, dotted and dashed lines.

i.e. we use Eq.(15) with  $\Gamma_f = 0$  which is obviously uncorrect but does not change the behavior of the solution in the relativistic regime. Using Eq.(22), (23) and (24) we finally get

$$P_{\text{diss}}(t) = \Phi(\lambda, \delta) \frac{\Gamma_0 M_s c^2}{\delta t_{\text{dec}}} \left( \frac{t}{t_{\text{dec}}} \right)^{-\left[ \frac{3\lambda+1+\lambda/\delta}{(2\lambda+1)} \right]} \quad (25)$$

where

$$\Phi(\lambda, \delta) = \frac{\lambda}{2} \left[ 1 - (2\lambda + 1)^{-1/2} \right]^2 \times (2\lambda + 1)^{\frac{1-\delta(1+4\lambda)}{2\delta(2\lambda+1)}}. \quad (26)$$

For  $\delta = 1$  and the two values of interest for  $\lambda$ , Eq.(25) becomes

$$\begin{aligned} \frac{P_{\text{diss}}}{\Gamma_0 M_s c^2 / t_{\text{dec}}} &= 6.6 \cdot 10^{-2} \left( \frac{t}{t_{\text{dec}}} \right)^{-7/4} \quad (\lambda = 3/2) \\ &= 1.5 \cdot 10^{-2} \left( \frac{t}{t_{\text{dec}}} \right)^{-3/2} \quad (\lambda = 1/2) \end{aligned} \quad (27)$$

which is in good agreement with the asymptotic behavior of the light curves shown in Fig.2.

#### 4 CAN THE REVERSE SHOCK CONTRIBUTE IN X-RAYS?

Despite their similarity with the SWIFT observations, it must remain clear that the profiles shown in Fig.2 only trace the power dissipated in the reverse shock. With the assumptions ordinary made to compute the reverse shock contribution in GRBs it should manifest itself mainly in the visible/IR range (Sari & Piran, 1999). Moreover most of the emission would

generally take place in the slow cooling regime so that the observed light curve will not necessarily trace the instantaneous energy release.

We therefore investigated whether, under some specific conditions, a substantial fraction of the dissipated power can be (i) radiated in the X-ray range and (ii) in the fast cooling regime. If the reverse shock contribution originates from synchrotron radiation of shock accelerated electrons, the characteristic synchrotron energy and cooling time behave as

$$E_s \propto B\Gamma_e^2 \quad \text{and} \quad t_s \propto B^{-2}\Gamma_e^{-1} \quad (28)$$

in the rest frame of the shocked material. Both the post-shock magnetic field  $B$  and typical electron Lorentz factor  $\Gamma_e$  have therefore to be large to produce an emission at high energy and on a short time scale  $t_s < t_{\text{dyn}}$ . An estimate of  $\Gamma_e$  is usually obtained assuming that a fraction  $\epsilon_e$  of the dissipated energy is injected into a fraction  $\zeta$  of the electrons so that

$$\Gamma_e \simeq \frac{\epsilon_e m_p}{\zeta m_e} e \quad (29)$$

where  $m_p$  and  $m_e$  are the proton and electron masses and  $ec^2$  is the energy dissipated per unit mass in the comoving frame. Similarly the post-shock magnetic field can be expressed as

$$B = \left(8\pi\epsilon_B \rho ec^2\right)^{1/2} \quad (30)$$

where  $\rho$  is the comoving density and  $\epsilon_B$  the fraction of the dissipated energy transferred to the magnetic field. To have large  $B$  and  $\Gamma_e$  values behind the shock we first supposed that a complete equipartition is established between the electronic, magnetic and baryonic components so that  $\epsilon_e = \epsilon_B = \epsilon_{\text{baryon}} = 1/3$ . We also assumed that only a small fraction  $\zeta \lesssim 10^{-2}$  of the electron population is accelerated in the shock. Adopting  $\zeta = 10^{-2}$  increases  $\Gamma_e$  by a factor of 100 and hence  $E_s$  by a factor  $10^4$  and decreases  $t_s$  by  $10^2$  compared to the standard  $\zeta = 1$  case.

The possibility to have only a small fraction of electrons being accelerated has already been considered by Bykov & Meszaros (1996) and also by Eichler & Waxman (2005) in the context of GRB afterglows. They showed that  $\zeta$  is not well constrained by the observations and, even if  $\zeta \sim 1$  appears slightly favored, they included the whole interval  $m_e/m_p < \zeta < 1$  in their analysis. In internal shocks, which are very similar to the reverse shock (both take place in the burst ejecta and are mildly relativistic) a large  $\epsilon_e$  is required to maintain a reasonable global efficiency since the fraction of the total energy dissipated by internal shocks hardly exceeds 10%. A small  $\zeta$  is also favored to insure that the emission takes place

in the gamma-ray range as shown by Daigne and Mochkovitch (1998) and more recently by Lee et al. (2005) in the context of the short hard burst GRB 050509b.

Examples of synthetic light curves in the XRT band 0.3 - 10 keV are shown in Fig.3 for the cases already considered in Fig.2. They have been obtained with  $\epsilon_e = \epsilon_B = 1/3$ ,  $\zeta = 10^{-2}$ , a slope  $p = 2.5$  for the electron energy distribution and an assumed redshift  $z = 2$ , typical of the SWIFT burst population. Especially in the wind case, they seem able to reproduce many of the observed XRT light curves. Conversely in the uniform density case we often obtain a depressed minimum followed by a bump rather than a continuous shallow evolution

## 5 DISCUSSION

Our proposal to explain the early X-ray afterglow of GRBs by a contribution of the reverse shock relies on three well defined assumptions: (*i*) the Lorentz factor of the material ejected at late times by the source has to decrease to small values,  $\Gamma_f < 10$ ; (*ii*) the shock dissipated energy must be transferred to only a small fraction of the electron population; and (*iii*) the forward shock contribution should lie below that of the reverse shock, at least during the first hours following burst trigger.

This last condition requires an ineffective transfer of energy to electrons ( $\epsilon_e \lesssim 10^{-2}$ ) or/and magnetic field ( $\epsilon_B \lesssim 10^{-5}$ ) in the material crossed by the forward shock. Difficulties to produce a sufficiently large magnetic field extending over the emitting region of GRB afterglows has for example been recently emphasized by Milosavljević & Nakar (2006). Then, if the reverse shock dominates in X-rays, what is the situation in the visible? We have checked that in most cases, taking small values of  $\epsilon_e$  or/and  $\epsilon_B$  in the forward shock, equally implies that the reverse shock dominates in the visible. The consistency of our proposal must therefore be checked not only with X-ray observations but also at lower wavelengths.

To better understand the multiwavelength behavior of the reverse shock contribution, we have computed the peak flux  $F_{\max}$  and the characteristic synchrotron and cooling frequencies  $\nu_m$  and  $\nu_c$  (Sari, Piran & Narayan, 1998). These three quantities depend on  $t$  (observer time),  $N_e$  (total number of shock accelerated electrons),  $B$  (magnetic field in shocked material),  $\Gamma_e$  (typical electron Lorentz factor) and  $\Gamma$  (Lorentz factor of the emitting material) in the following way

$$\begin{aligned}
F_{\max} &\propto \Gamma B N_e \\
\nu_m &\propto \Gamma \Gamma_e^2 B \\
\nu_c &\propto \Gamma^{-1} B^{-3} t^{-2}
\end{aligned} \tag{31}$$

We consider their temporal evolution in the asymptotic regime already described in Sect.3.2, assuming a wind environment. The evolution of  $\Gamma$  is given by Eq.(22) which can be re-expressed as

$$\Gamma(t) = \Gamma_0 \left( \frac{t}{2t_{\text{dec}}} \right)^{-1/4} = 119 \Gamma_2 \left( \frac{t}{t_{\text{dec}}} \right)^{-1/4} \tag{32}$$

where  $\Gamma_2 = \Gamma_0/100$ . Eq.(18), (23) and (29) show that  $\Gamma_e$  reaches a constant value

$$\Gamma_e = 4.3 \cdot 10^{-2} \frac{m_p}{m_e} \frac{\epsilon_e}{\zeta} \frac{p-2}{p-1} = 79 \frac{\epsilon_e}{\zeta} \frac{p-2}{p-1} \tag{33}$$

where we have added the normalizing factor  $\frac{p-2}{p-1}$  ( $p$  being the slope of the relativistic electron distribution) which was not present in Eq.(29). For the magnetic field, instead of Eq.(30) it is easier to use the continuity of the energy density at the contact discontinuity which yields

$$B = (32\pi\epsilon_B c^2 A)^{1/2} \frac{\Gamma}{R} \tag{34}$$

where  $A$  is the wind constant such as  $\rho(R) = A/R^2$  ( $A = 5 \cdot 10^{11} A_*$ ). With Eq.(20) for  $R$  and Eq.(32) for  $\Gamma$  we get

$$B(t) = 3 \cdot 10^4 \frac{(\epsilon_B A_*)^{1/2}}{t_{\text{dec}} \Gamma_2} \left( \frac{t}{t_{\text{dec}}} \right)^{-3/4} \text{ G} \tag{35}$$

Finally, the number of accelerated electrons can be obtained from Eq.(24) which, for  $\delta = 1$ , gives

$$N_e(t) = \frac{2\zeta E_s}{\Gamma_0 m_p c^2} \left[ 1 - 1.19 \left( \frac{t}{t_{\text{dec}}} \right)^{-1/4} \right] \tag{36}$$

where  $E_s = \frac{1}{2}\Gamma_0 M_s c^2$  is the total energy in the slow material. From Eq.(32), (33), (35) and (36) the expressions for  $F_{\max}$ ,  $\nu_m$  and  $\nu_c$  can be computed

$$\begin{aligned}
F_{\max} &= 1.4 \cdot 10^8 \frac{(1+z)}{D_{28}^2} \frac{(\zeta E_{53})(\epsilon_B A_*)^{1/2}}{\Gamma_2} \times \frac{1}{t} \text{ mJ} \\
\nu_m &= 9.15 \cdot 10^{16} (\epsilon_B A_*)^{1/2} \left( \frac{\epsilon_e}{\zeta} \right)^2 \left( \frac{p-2}{p-1} \right)^2 \times \frac{1}{t} \text{ Hz} \\
\nu_c &= 8.2 \cdot 10^8 \frac{t_{\text{dec}}^{1/2} \Gamma_2^2}{(\epsilon_B A_*)^{3/2}} \times t^{1/2} \text{ Hz}
\end{aligned} \tag{37}$$

with  $E_{53} = E_s/10^{53}$  erg and where the expression for  $F_{\max}$  has been written in the limit  $t \gg t_{\text{dec}}$ . Compared to the forward shock case, it can be seen that  $F_{\max} \propto t^{-1}$  and that  $\nu_m$  decays less rapidly (as  $t^{-1}$  instead of  $t^{-3/2}$ ). For a wind environment, the cooling frequency has the same power law dependence,  $\nu_c \propto t^{1/2}$ . From these expressions the flux can be

computed for the different possible radiative regimes (Sari, Piran & Narayan, 1998), the results being given in Appendix A.

Let us for example take the following values of the parameters:  $\Gamma_2 = 1$ ,  $\epsilon_e = \epsilon_B = 0.33$ ,  $\zeta = 10^{-2}$ ,  $p = 2.5$ ,  $A_* = 0.5$  and  $t_{\text{dec}} = 100$  s. Then, the transition from fast to slow cooling occurs at  $t = 1.3(1+z)$  day. Now adopting 1 keV and 2 eV as typical energies for the X-ray and visible bands (i.e.  $\nu_X = 2.4 \cdot 10^{17}$  Hz and  $\nu_V = 4.8 \cdot 10^{14}$  Hz) and a redshift  $z = 2$ , it appears that after only a few seconds  $\nu_X$  becomes larger than  $\nu_m$  and then remains larger than  $\nu_c$  in the slow cooling regime. The corresponding temporal slope is  $\alpha_X = (2p+1)/4 = 1.5$ . At the visible frequency, we initially have  $\nu_c < \nu_V < \nu_m$  and therefore  $\alpha_V = 0.75$ . The visible frequency crosses  $\nu_m$  at  $t = 2.6$  h (in the fast cooling regime) and then  $\nu_c$  (in slow cooling) at very late times. A break from  $\alpha_V = 0.75$  to 1.5 is expected at  $t = 2.6$  h.

Since these predicted slopes are only valid in the asymptotic regime where  $t \gg t_{\text{dec}}$  we have performed a numerical simulation with the burst parameters given above except for the fraction  $\zeta$  of accelerated electrons which is varied between 0.003 and 0.03. We assume in addition that  $E_{53} = 1$  and adopt a rest frame reddening  $A_V = 0.5$  in the burst host galaxy. The resulting X-ray and visible light curves are shown in Fig.4. For  $\zeta = 3 \cdot 10^{-3}$  and  $10^{-2}$  they exhibit chromatic breaks. The break in X-rays is a consequence of the dynamics of the reverse shock (it is already present in the bolometric light curve) while the break in the visible is a spectral break (when  $\nu_V$  crosses  $\nu_m$ ). The cases with  $\zeta = 3 \cdot 10^{-3}$ ,  $10^{-2}$  and  $3 \cdot 10^{-2}$  are very similar to the early afterglow light curves of respectively GRB 050802, GRB 050922c and GRB 050801 (see Panaitescu et al, 2006 and Panaitescu, 2006).

The subsequent evolution of the afterglow will depend on the behavior of  $\epsilon_e$  and  $\epsilon_B$  in the forward shock. If they increase enough with time the forward shock contribution will eventually dominate but the moment of the transition is difficult to estimate in the absence of any reliable physical model for the possible variations of the shock microphysics parameters. If the forward shock takes over after about one day, the multiwavelength fits of GRB afterglows obtained in the pre-SWIFT era will remain valid but the early afterglow will be explained by the reverse shock. At the transition, a change of slope or the presence of a bump may however be expected. While such accidents have been observed in some bursts they do not seem to be a generic feature of GRB afterglows.

A much more radical point of view can still be adopted: it would to suppose that in some cases the forward shock never takes over so that the afterglow is entirely produced by the reverse shock! The results shown in Fig.4 seem to indicate that this possibility should not be

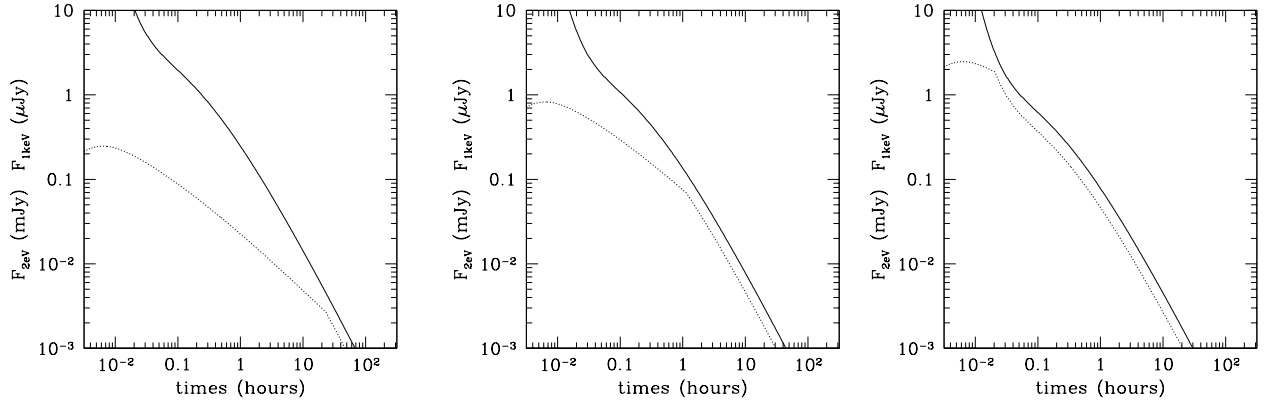


**Figure 4.** Early afterglow light curves produced by the reverse shock for  $\epsilon_e = \epsilon_B = 0.33$ ,  $p = 2.5$ ,  $\Gamma_2 = 1$ ,  $A_* = 0.5$ ,  $t_{\text{dec}} = 100$  s,  $A_V = 0.5$  and, from left to right,  $\zeta = 3 \cdot 10^{-3}$ ,  $10^{-2}$  and  $3 \cdot 10^{-2}$  (see text for details). The full (resp. dotted) line is the X-ray (resp. the visible) afterglow. Compare these results to the early afterglow light curves of respectively GRB 050802, GRB 050922c and GRB 050801 as shown in Panaitescu (2006).

excluded a priori even if, clearly, considerable work will be needed to confirm it. As for the forward shock hypothesis it will have to be confronted to a large amount of multiwavelength afterglow data and show that it can provide a consistent picture for their interpretation.

## 6 CONCLUSION

We have developed a simplified model which enabled us to follow simultaneously the dynamics of the internal, external and reverse shocks in GRBs. We were mainly interested by dissipation in the reverse shock when the Lorentz factor in the material which is ejected at late times by the source decreases to small values,  $\Gamma_f < 10$ . The propagation of the reverse shock then extends over quite a long time needed to decelerate the fast moving part of the ejecta down to  $\Gamma \sim \Gamma_f$ . We have obtained the dissipated power as a function of observed time for different burst environments (wind or constant density). Its evolution shows a striking resemblance with the early afterglow light curves observed by SWIFT, especially in the wind case. However the reverse shock contribution is normally expected at low energy and to appear in X-rays it requires a transfer of the dissipated power to only a small fraction ( $\zeta \lesssim 10^{-2}$ ) of the electron population. If this is possible, SWIFT XRT observations could be better explained by the reverse shock than by the standard afterglow produced by the forward shock.

We have also computed the optical emission from the reverse shock. The comparison with the X-ray light curve often reveals the presence of chromatic breaks during the first hours. Such breaks have been observed and are difficult to explain with the standard model

where the afterglow comes from the forward shock. We have finally even proposed that in some cases the entire afterglow could be produced by the reverse shock. We fully understand that, to be validated, this non standard view still has to show that it can successfully explain multiwavelength observations of a reasonable sample of GRB afterglows. We aim to perform these necessary tests in a work in preparation.

## APPENDIX A:

Using Eq.(37) for  $F_{\max}$ ,  $\nu_m$  and  $\nu_c$  we give the expressions for the flux at a given frequency in the fast and slow cooling regimes:

*Fast cooling*

1)  $\nu < \nu_c$

$$\begin{aligned} F_\nu &= F_{\max} \left( \frac{\nu}{\nu_c} \right)^{1/3} \\ &= 10^{11} \frac{(1+z)^{4/3}}{D_{28}^2} \frac{(\zeta E_{53})(\epsilon_B A_*)}{t_{\text{dec}}^{1/6} \Gamma_2^{5/3}} \nu_{17.4}^{1/3} \times t^{-7/6} \text{ mJ} \end{aligned} \quad (\text{A1})$$

2)  $\nu_c < \nu < \nu_m$

$$\begin{aligned} F_\nu &= F_{\max} \left( \frac{\nu}{\nu_c} \right)^{-1/2} \\ &= 7.7 \cdot 10^3 \frac{(1+z)^{1/2}}{D_{28}^2} \frac{(\zeta E_{53}) t_{\text{dec}}^{1/4}}{(\epsilon_B A_*)^{1/4}} \nu_{17.4}^{-1/2} \times t^{-3/4} \text{ mJ} \end{aligned} \quad (\text{A2})$$

3)  $\nu > \nu_m$

$$\begin{aligned} F_\nu &= F_{\max} \left( \frac{\nu_m}{\nu_c} \right)^{-1/2} \left( \frac{\nu}{\nu_m} \right)^{-p/2} \\ &= 1.3 \cdot 10^4 \times 0.36^{p/2} \frac{(1+z)^{1-p/2}}{D_{28}^2} (\zeta E_{53}) (\epsilon_B A_*)^{\frac{p-2}{4}} t_{\text{dec}}^{1/4} \\ &\quad \times \left( \frac{\epsilon_e}{\zeta} \right)^{p-1} \left( \frac{p-2}{p-1} \right)^{p-1} \nu_{17.4}^{-p/2} \times t^{-\frac{2p+1}{4}} \text{ mJ} \end{aligned} \quad (\text{A3})$$

*Slow cooling*

1)  $\nu < \nu_m$

$$\begin{aligned} F_\nu &= F_{\max} \left( \frac{\nu}{\nu_m} \right)^{1/3} \\ &= 2 \cdot 10^8 \frac{(1+z)^{4/3}}{D_{28}^2} \frac{(\zeta E_{53})(\epsilon_B A_*)^{1/3}}{\Gamma_2} \\ &\quad \times \left( \frac{\epsilon_e}{\zeta} \right)^{-2/3} \left( \frac{p-2}{p-1} \right)^{-2/3} \nu_{17.4}^{1/3} \times t^{-2/3} \text{ mJ} \end{aligned} \quad (\text{A4})$$

2)  $\nu_m < \nu < \nu_c$ 

$$\begin{aligned}
F_\nu &= F_{\max} \left( \frac{\nu}{\nu_m} \right)^{\frac{1-p}{2}} \\
&= 1.4 \cdot 10^8 \times 0.36^{\frac{p-1}{2}} \frac{(1+z)^{\frac{3-p}{2}} (\zeta E_{53}) (\epsilon_B A_*)^{\frac{p+1}{4}}}{D_{28}^2 \Gamma_2} \\
&\times \left( \frac{\epsilon_e}{\zeta} \right)^{p-1} \left( \frac{p-2}{p-1} \right)^{p-1} \nu_{17.4}^{(1-p)/2} \times t^{-\frac{p+1}{2}} \text{ mJ}
\end{aligned} \tag{A5}$$

3)  $\nu > \nu_c$ 

$$\begin{aligned}
F_\nu &= F_{\max} \left( \frac{\nu_m}{\nu_c} \right)^{\frac{p-1}{2}} \left( \frac{\nu}{\nu_c} \right)^{-\frac{p}{2}} \\
&= 1.3 \cdot 10^4 \times 0.36^{p/2} \frac{(1+z)^{1-p/2}}{D_{28}^2} (\zeta E_{53}) (\epsilon_B A_*)^{\frac{p-2}{4}} t_{\text{dec}}^{1/4} \\
&\times \left( \frac{\epsilon_e}{\zeta} \right)^{p-1} \left( \frac{p-2}{p-1} \right)^{p-1} \nu_{17.4}^{-p/2} \times t^{-\frac{2p+1}{4}} \text{ mJ}
\end{aligned} \tag{A6}$$

In all these expressions the frequency (in observer frame) is in unit of  $10^{17.4}$  Hz, corresponding to 1 keV.

## ACKNOWLEDGMENTS

The authors would like to thank John Eldridge for a careful reading of the manuscript.

## REFERENCES

- Beloborodov, A.M. 2002, ApJ, 565, 808.
- bibitem[Bykov & Meszaros] Bykov, A.M., & Meszaros, P. 1996, ApJ, 461, L37.
- Burrows D.N., Hill, J.E., Nousek, J.A. et al. 2005a, SSRv, 120, 165.
- Burrows D.N., Romano, P., Falcone A. et al. 2005b, Science, 309, 1833.
- Daigne, F., & Mochkovitch, R. 1998, MNRAS, 296, 275.
- Daigne, F., & Mochkovitch, R. 2000, A&A, 358, 1157.
- Daigne, F., & Mochkovitch, R. 2003, MNRAS, 342, 587.
- Eichler, D., Granot, J. 2005, ApJ, 641, L5.
- Eichler, D., Waxman, E. 2005, ApJ, 627, 861.
- Fan, Y.Z. & Piran, T. 2006, MNRAS, 369, 197.
- Fan, Y.Z. & Wei, D.M. 2005, MNRAS, 364, L42.
- Granot, J., Piran, T. & Sari, R. 1999, ApJ, 513, 679.
- Kobayashi, S., Piran, T. & Sari, R. 1997, ApJ, 490, 92.
- Kumar, P. & Panaitescu, A. 2000, ApJ, 541, 51.
- Lee, W.H., Ramirez-Ruiz, E. & Granot, J. 2005, ApJ, 630, L165.
- Madau, P. & Thompson, C. 2000, ApJ, 534, 239.
- Milosavljević, M. & Nakar, E. 2006, ApJ, 641, 978.
- Nousek, J.A., Kouveliotou, C., Grupe, D. et al. 2005, ApJ 642, 389.

- Panaitescu, A., Meszaros, P., Gehrels, N. et al. 2005, MNRAS, 366, 1357.
- Panaitescu, A. 2006, astro-ph/0607396.
- Panaitescu, A., Meszaros, P., Burrows, D. et al. 2006, MNRAS, 369, 2059.
- Ryde, F. & Svensson, R. 2000, ApJ, 529, L13.
- Sari, R., & Piran, T. 1999, ApJ, 517, L109.
- Sari, R., Piran, T. & Narayan, R. 1998, ApJ, 497, L17.
- Soderberg, A.M., Fenimore, E.E. 2001, in *Gamma-Ray Bursts in the Afterglow Era*, Edited by Enrico Costa, Filippo Frontera, and Jens Hjorth. Berlin Heidelberg: Springer, 2001, p. 87.
- Rees, M.J., & Meszaros, P. 1994, ApJ, 430, L93.
- Tagliaferri, G, Goad, M, Chincarini, G. et al. 2005, Nature, 436, 985.
- Thompson, C., & Madau, P. 2000, ApJ, 538, 105.
- Woods, E., & Loeb, A. 1999, ApJ, 523, 187.
- Zhang, B., Kobayashi, S. 2005, ApJ 628, 315.
- Zhang, B., Fan, Y.Z., Dyks, J. et al. 2005, ApJ 642, 354.
- Zhang, B., Liang, E., Page, K.L. et al. 2006, astro-ph/0610177.